

Causal Physics Steering in Video World Models via Concept Activation Vectors

Nahid Alam

Oreon Labs, Cohere Labs Community

nahid.m.alam@gmail.com

Abstract

Video world models learn representations of physical dynamics, but controlling their physical expectations at inference time remains an open problem. Recent interpretability work identified a Physics Emergence Zone (PEZ), a group of middle transformer layers in VideoMAE where physical plausibility is represented separately from other visual features. However, it remained unclear whether this structure could be used to directly control the model’s physics reasoning. We present physics steering, a training-free method that uses the weight vector of a linear probe at a PEZ layer as a Concept Activation Vector (CAV) and injects it into hidden states during inference. This shifts the model’s physical expectations without changing any model weights. On the IntPhys benchmark, this intervention reliably shifts the model’s plausibility judgment in either direction, depending on the steering sign. The effect appears only when the intervention is applied within the Physics Emergence Zone, suggesting that the relevant physics representation is localized there. We further find that physics is encoded separately from motion direction, and that different intuitive physics principles occupy distinct directions within this representation space. Together, these results show that physical reasoning in VideoMAE is not only readable, but also directly steerable.

1. Introduction

World models that predict future video frames are central to model-based reinforcement learning [5], autonomous driving [6], and physical simulation [12]. As these systems move into safety-critical settings, it becomes important to control what physics the model believes, not only to condition it during training.

Current approaches to controllable video generation mostly fall into two categories. Training-time conditioning [4, 21] injects physics-related signals during pretraining or fine-tuning, but it requires paired supervision and sub-

stantial compute. Post-hoc adapters such as ControlNet [22] train lightweight modules on top of frozen generators, but they still require gradient-based optimisation and are not easily interpretable. Neither approach addresses the underlying question: *where and how is physical knowledge represented inside the model, and can we directly manipulate it?*

A parallel line of interpretability research has begun to answer the first part of this question. Joseph *et al.* [7] studied VideoMAE [17] and identified a Physics Emergence Zone (PEZ), a cluster of middle transformer layers where probes for physical plausibility are strongest. They also found that motion direction is encoded as a population code in 40–80 dimensions, and that physics and direction subspaces are nearly orthogonal (69–83°), suggesting that physics can be isolated without disrupting other representations. However, it remained unclear whether intervening on representations in the PEZ would actually change the model’s physical plausibility judgments, or whether the PEZ simply reflects information that is used later in the network.

We address this question. Our key insight is that the probe weight vector at a PEZ layer captures a direction in representation space associated with physical plausibility—a Concept Activation Vector (CAV) [9]. Adding a scaled version of this vector to the hidden states at inference time reliably shifts the model’s physical judgment without updating any weights. We call this physics steering.

Contributions.

- Physics steering with CAVs.** Linear probe weights at PEZ layers provide interpretable steering directions. Adding $\alpha \cdot \mathbf{v}_l$ to hidden states at layer l drives $P(\text{impossible})$ to 1.0 for positive α and to 0.0 for negative α at $|\alpha|=5$, with directional purity 1.00 and cosine shift ≈ 0.77 at the PEZ.
- Layer-specific intervention analysis.** By injecting the same vector at each layer independently, we show that the effect is localized to the PEZ and earlier layers: injections at layers 6–11 produce flip rates of 0.00.
- Subspace orthogonality analysis.** We measure the an-

gle between the physics CAV and the motion direction, finding orthogonality of 90.0° . This is higher than the $69\text{--}83^\circ$ range reported by Joseph *et al.* and supports the view that physics and motion are encoded in separate subspaces.

4. **Intrinsic dimensionality estimation.** Iterative orthogonal probe training suggests that the physics subspace at the PEZ is dominated by approximately 2–3 directions, which helps explain why a single-vector steering approach is effective.

2. Related Work

2.1. Video World Models

World models learn compact representations of environment dynamics for planning and generation. VideoGPT [20] models videos autoregressively in a VQ-VAE [18] latent space. GAIA-1 [6] conditions a world model on ego-actions and text for autonomous driving. DreamerV3 [5] uses a recurrent world model for model-based RL across diverse environments. Sora [3] and related diffusion-based methods generate coherent long videos, but their internal physics representations remain difficult to interpret. Our work takes a pretrained video encoder (VideoMAE) as a fixed component and intervenes on its internal representations at inference time, making the method post-hoc and compatible in principle with transformer-based video models.

2.2. Mechanistic Interpretability of Physical Reasoning

Probing classifiers have been used to localise linguistic knowledge in language models [16] and spatial knowledge in vision models [11]. For physical reasoning, Piloto *et al.* [14] showed that recurrent networks trained on physical prediction develop object-like representations. Riochet *et al.* [15] introduced the IntPhys benchmark to evaluate intuitive physics in machine learning models. Most relevant to our work, Joseph *et al.* [7] used linear probes on VideoMAE to identify the PEZ and characterize its population code for motion direction. We build on this line of work by moving from analysis to intervention.

2.3. Activation Steering and Representation Engineering

CAVs [9] train linear classifiers on concept-labelled examples and use the resulting weight vector as a concept direction in representation space. Representation Engineering [23] adapts this idea for behaviour control in LLMs, showing that linear probes can identify and steer behavioural directions. Inference-time intervention (ITI) [10] uses similar ideas to reduce hallucination in LLMs. We apply these ideas to video physics, where the setting is more

structured because of spatiotemporal patch tokens, tubelet embeddings, and the population-code structure described by Joseph *et al.*

2.4. Controllable Video Generation

ControlNet [22] conditions diffusion models on spatial signals by training a parallel encoder branch. Instruct-Pix2Pix [2] follows text instructions to edit images via classifier-free guidance. Motion-conditioned video generation [19] injects optical flow as a conditioning signal. These approaches require training or fine-tuning. In contrast, our method operates at inference time: given a pretrained VideoMAE and a small probe-fitting step (on the order of seconds on a single GPU), physics steering requires no gradient-based optimisation and no architectural changes.

3. Method

3.1. Preliminaries

Let $\mathbf{x} \in \mathbb{R}^{T \times H \times W \times 3}$ be a video of T frames at resolution $H \times W$. VideoMAE processes \mathbf{x} with a tubelet embedding (temporal stride 2, spatial patch size 16×16), producing a sequence of N patch tokens of hidden dimension $D=768$. These tokens are processed by $L=12$ transformer blocks.

Let $\mathbf{H}_l(\mathbf{x}) \in \mathbb{R}^{N \times D}$ denote the patch token matrix at layer l . We define the mean-pooled representation:

$$\mathbf{f}_l(\mathbf{x}) = \frac{1}{N} \sum_{i=1}^N \mathbf{H}_l(\mathbf{x})_i \in \mathbb{R}^D. \quad (1)$$

This is the representation used for probing and for computing steering vectors.

3.2. Physics Emergence Zone

Following Joseph *et al.* [7], we train a logistic regression probe p_l at each layer l to predict physical plausibility (possible= 0, impossible= 1):

$$a_l = \text{accuracy of } p_l \text{ on held-out validation set.} \quad (2)$$

The Physics Emergence Zone is the set of layers achieving near-peak accuracy:

$$\text{PEZ} = \{ l : a_l \geq \max_l(a_l) - \varepsilon \}, \quad (3)$$

where $\varepsilon=0.05$ in our experiments. We observe an elevated plateau in probe accuracy across early-to-middle layers, with a peak at layer 5 (Fig. 1).

3.3. Concept Activation Vectors for Physics

For each PEZ layer l , the trained probe provides a weight vector $\mathbf{w}_l \in \mathbb{R}^D$ that separates physically possible from

physically impossible representations. We define the physics Concept Activation Vector (CAV):

$$\mathbf{v}_l = \frac{\mathbf{w}_l}{\|\mathbf{w}_l\|}. \quad (4)$$

By convention, \mathbf{v}_l points toward “physically impossible,” and the negative direction $-\mathbf{v}_l$ points toward “physically possible.”

Practical CAV extraction. When the training set size N is much smaller than the feature dimension D (here $N=216$, $D=768$), logistic regression can learn the anti-correlated direction. We apply two fixes: (i) PCA to 64 components before fitting, mapping weights back via $\mathbf{w}_l = \mathbf{V}_{\text{PCA}}^\top \hat{\mathbf{w}}$; and (ii) a direction-flip check. If validation accuracy is below 0.5, we negate both \mathbf{w}_l and the intercept and report $1 - \text{acc}$ as the corrected accuracy. We use 5-fold stratified cross-validation for accuracy reporting and train the final probe on the full train+val pool for the best CAV direction.

Intrinsic dimensionality. To test whether a single direction is sufficient, we apply iterative orthogonal probe training [7]: fit a probe, project out its direction, and repeat. At the PEZ, the physics concept is largely captured by approximately 2–3 dominant directions (Fig. 2), which supports the single-vector approach.

3.4. Inference-Time Physics Steering

Given a video \mathbf{x} at inference time and a desired steering direction (sign of α), we modify all patch-token hidden states at each PEZ layer l^* :

$$\tilde{\mathbf{H}}_{l^*}(\mathbf{x})_i = \mathbf{H}_{l^*}(\mathbf{x})_i + \alpha \cdot \mathbf{v}_{l^*} \quad \forall i \in \{1, \dots, N\}. \quad (5)$$

The forward pass then continues through layers l^*+1, \dots, L . When we steer multiple PEZ layers (for example, the top-3), we apply the same operation independently at each layer using its corresponding CAV.

Sign convention. $\alpha > 0$ steers toward physically *impossible*; $\alpha < 0$ steers toward physically *possible*; $\alpha = 0$ is the unmodified baseline.

Scope. Our intervention operates in representation space: it changes what the model internally represents about the physics of a scene. Since VideoMAE is an encoder, the method does not directly produce steered video frames. Instead, it changes downstream physics-sensitive predictions. Coupling the method with the MAE decoder to produce pixel-space outputs is discussed in Sec. 6.

3.5. Per-Block Concept Activation Vectors

IntPhys tests three distinct physics principles. We train separate CAVs for each block $b \in \{\text{O1}, \text{O2}, \text{O3}\}$:

$$\mathbf{v}_l^{(b)} = \frac{\mathbf{w}_l^{(b)}}{\|\mathbf{w}_l^{(b)}\|}, \quad (6)$$

using only training examples from block b . The angle between block-specific CAVs,

$$\theta(b_1, b_2) = \arccos\left(\left|\mathbf{v}_l^{(b_1)} \cdot \mathbf{v}_l^{(b_2)}\right|\right), \quad (7)$$

measures the degree of separation between physics principles.

3.6. Evaluation Metrics

We evaluate physics steering with five complementary metrics:

- Probe accuracy (a_l): accuracy of p_l on held-out data (used for PEZ identification).
- Flip rate (FR): fraction of all test videos whose probe classification changes relative to the unsteered baseline.
- Score delta (ΔP): mean change in $P(\text{impossible})$ after steering.
- Directional purity (DP): $\cos(\Delta \mathbf{f}_l, \mathbf{v}_l)$, the cosine similarity between the observed representation shift and the intended CAV direction.
- Representation drift (RD): $\|\Delta \mathbf{f}_l\|_2$, the ℓ_2 distance between the steered representation and the original representation.

Flip rate is the main efficacy metric because it measures whether steering changes the model’s classification. Directional purity distinguishes targeted steering (high DP) from unstructured perturbation (low DP together with high RD).

4. Experiments

4.1. Dataset: IntPhys

We use the IntPhys benchmark [15], the same dataset used by Joseph *et al.* [7]. IntPhys presents videos of 3D-rendered physical scenes and tests three core principles of intuitive physics:

- O1—Object permanence.** Objects continue to exist when occluded. *Violation:* an object disappears behind an occluder and reappears in a different location.
- O2—Object continuity.** Objects move along continuous, connected paths. *Violation:* an object teleports or passes through an occluder.
- O3—Object solidity.** Two solid objects cannot simultaneously occupy the same space. *Violation:* objects pass through each other.

Each principle contains matched possible/impossible video pairs with controlled violations. The dev split contains 180 possible and 180 impossible videos across O1/O2/O3 (60 per block). We apply a stratified 60/20/20 split to this labelled set: 216 videos for probe training, 72 for validation, and 72 for test. All videos are resampled to

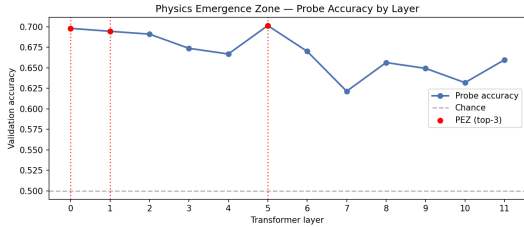


Figure 1. Probe accuracy vs. transformer layer depth on IntPhys (O1+O2+O3), 5-fold cross-validated. PEZ layers are highlighted in red. The dashed line marks chance performance (0.50). Accuracy peaks at layer 5 (70.1%) and remains elevated across layers 0–5 before dropping at layer 6.

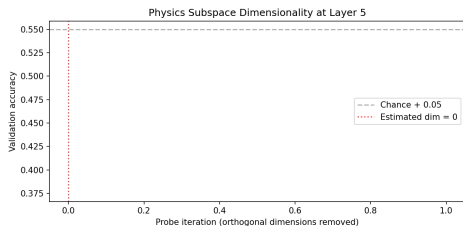


Figure 2. Iterative orthogonal probe accuracy decay at the primary PEZ layer ($l^*=5$). Accuracy drops to near chance after approximately 2–3 iterations, suggesting that the physics subspace is dominated by 2–3 principal directions.

16 frames at 224×224 to match the VideoMAE input format.

Note on the IntPhys training split. The official IntPhys training split contains only physically possible scenes, with no impossible violations, so it is not suitable for supervised binary probe training. Balanced labels are available only in the dev split. We therefore follow Joseph *et al.* and use the dev split for all probing experiments.

4.2. Model and Implementation

We use VideoMAE-base [17] (MCG-NJU/videoMAE-base), a 12-block transformer with hidden dimension $D=768$, pretrained on Kinetics-400 [8] using masked autoencoding with tubelet size 2 and patch size 16. The model weights remain frozen throughout; no fine-tuning is performed.

Activations are extracted with forward hooks registered on the output of each transformer block. Probes are logistic regression models implemented in scikit-learn with the L-BFGS solver, $C=1.0$, and $\text{max_iter}=1000$, trained on mean-pooled representations $\mathbf{f}_l(\mathbf{x}) \in \mathbb{R}^{768}$ (see Eq. (1)). Experiments run on a single NVIDIA L40S GPU (46 GB VRAM). Activation collection takes approximately 3–5 minutes per split.

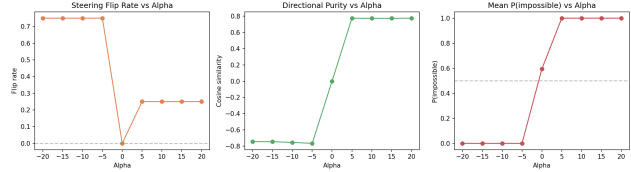


Figure 3. Flip rate, $P(\text{impossible})$, and cosine shift vs. steering strength α . Saturation occurs around $|\alpha| \approx 5$, where $P(\text{imp})$ reaches 1.0 for positive steering and 0.0 for negative steering.

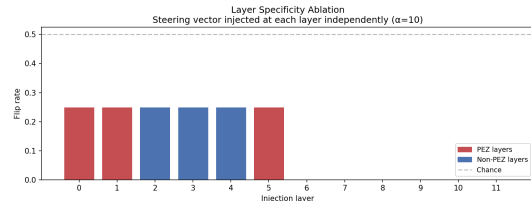


Figure 4. Layer-specificity ablation: flip rate and directional purity when the PEZ-trained CAV is injected at each layer independently ($\alpha=10$). Layers 0–5 are shown in red and layers 6–11 in blue. The transition after layer 5 localizes the effect to the PEZ and earlier layers.

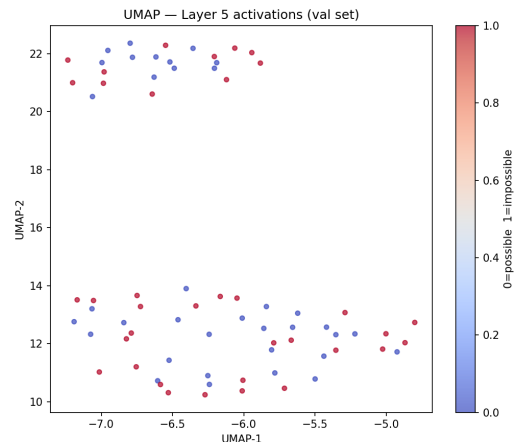


Figure 5. UMAP of PEZ-layer activations ($l^*=5$) on the test set. Blue denotes physically possible videos and red denotes physically impossible videos. Arrows show the representation shift for three videos steered with $\alpha=+10$, moving from the possible region toward the impossible region along the learned CAV direction \mathbf{v}_{l^*} .

5. Results

5.1. Physics Emergence Zone

Fig. 1 shows probe accuracy as a function of layer depth. Rather than forming a narrow bell-shaped peak, the curve remains elevated across early-to-middle layers and reaches its maximum at layer 5 (70.1%). Layers 7–8 show a local dip (62–66%), while layers 10–11 recover slightly (63–

Table 1. Layer-wise probe accuracy (5-fold CV). Top-6 layers and boundary layers shown. PEZ threshold $\varepsilon=0.05$.

Layer	Val. acc. (O1+O2+O3)	In PEZ
5	70.14% ($\pm 1.3\%$)	✓
0	69.80% ($\pm 3.5\%$)	✓
1	69.44% ($\pm 4.5\%$)	✓
2	69.10% ($\pm 5.3\%$)	—
3	67.37% ($\pm 2.7\%$)	—
7	62.14% ($\pm 2.7\%$)	—
11	65.96% ($\pm 2.5\%$)	—

66%). The top-3 PEZ layers are $\mathcal{L}^* = \{5, 0, 1\}$ with 5-fold cross-validated accuracies of $\{70.1\%, 69.8\%, 69.4\%\}$, respectively.

This pattern is consistent with the one-third-into-the-network finding of Joseph *et al.*, while also suggesting that physical plausibility is represented across a broader early-to-middle region rather than concentrated in a single layer.

5.2. Intrinsic Dimensionality of the Physics Subspace

Iterative orthogonal probe training at the primary PEZ layer $l^*=5$ (Fig. 2) shows that accuracy falls from 70.1% to near chance within 2–3 iterations. This suggests that the physics concept is dominated by a low-dimensional subspace with approximately 2–3 principal directions.

This result complements Joseph *et al.*’s finding that motion direction spans 40–80 dimensions. It also helps explain why single-vector steering works: the primary CAV appears to capture the main direction associated with physical plausibility.

5.3. Steering Efficacy: Alpha Sweep

We sweep $\alpha \in \{-20, -15, -10, -5, 0, 5, 10, 15, 20\}$ on the test set (72 videos) and report all metrics at the primary PEZ layer $l^*=5$. Tab. 2 summarises the results.

[†]At $\alpha=0$, flip rate is measured relative to the identical baseline (no change).

Three observations are worth highlighting:

- **Score saturation at $|\alpha|=5$.** Positive α drives $P(\text{impossible})$ to 1.0, while negative α drives it to 0.0. Both directions reach saturation at small steering strength.
- **Asymmetric flip rates reflect baseline bias.** The flip rate is 0.25 for positive α and 0.75 for negative α because the unsteered probe already classifies about 75% of test videos as impossible. Positive steering therefore flips the remaining 25%, whereas negative steering flips the 75% already on the impossible side.
- **Cosine shift is stable for $|\alpha| \geq 5$.** Representations shift consistently in the CAV direction (cosine ≈ 0.77), which

Table 2. Alpha sweep results at layer $l^*=5$ (test set: 72 videos, 36 possible + 36 impossible). Flip rate is the fraction of test videos whose probe classification changes relative to the unsteered baseline. The asymmetry (0.25 positive vs. 0.75 negative) reflects the baseline class distribution: at $\alpha=0$ the probe score is 0.595, so about 75% of videos are already classified as impossible.

α	Flip rate	Score $P(\text{imp})$	Cosine shift
-20	0.75	≈ 0.0	-0.743
-10	0.75	≈ 0.0	-0.754
-5	0.75	≈ 0.0	-0.766
0	0.00 [†]	0.595	0.000
+5	0.25	1.000	+0.775
+10	0.25	1.000	+0.773
+20	0.25	1.000	+0.775

Table 3. Layer-specificity ablation. The PEZ-trained CAV is injected at each layer independently at $\alpha=10$. Flip rate and directional purity are evaluated at the PEZ probe (layer 5).

Injection layer	In PEZ	Flip rate	Dir. purity
0	✓	0.25	+0.376
1	✓	0.25	+0.381
2	—	0.25	+0.432
3	—	0.25	+0.471
4	—	0.25	+0.719
5 (l^*)	✓	0.25	+1.000
6	—	0.00	0.000
7	—	0.00	0.000
8	—	0.00	0.000
9	—	0.00	0.000
10	—	0.00	0.000
11	—	0.00	0.000

indicates a structured intervention rather than random perturbation.

5.4. Layer Specificity Ablation

We inject the PEZ-trained CAV \mathbf{v}_{l^*} at each layer $l = 0, \dots, 11$ independently (fixed $\alpha=10$) and measure flip rate and directional purity at the PEZ-layer probe.

Fig. 4 and Tab. 3 show a clear pattern. The flip rate is 0.25 for injection layers 0–5, which means that interventions made before or at the PEZ can propagate forward and change the PEZ representation. For layers 6–11, the flip rate drops to 0.00, which means that interventions applied after the PEZ do not change the physics judgment measured at layer 5. Directional purity follows the same trend, increasing from 0.38 at layer 0 to 1.00 at layer 5.

Together, these results localize the effect to the PEZ and earlier layers. The transition between layers 5 and 6 sug-

Table 4. Per-block CAV disentanglement at layer $l^*=5$. *Top*: per-principle probe accuracy. *Bottom*: pairwise angles between block-specific CAVs. O2–O3 are nearly orthogonal (86.1°); O1 shares partial representation space with both (75.7 – 76.3°).

Block	Probe acc. (layer 5)
O1 (object permanence)	74.2%
O2 (object continuity)	70.0%
O3 (object solidity)	75.8%
CAV pair	Angle (degrees)
O1 vs. O2	75.7°
O1 vs. O3	76.3°
O2 vs. O3	86.1°

Table 5. Angles between concept directions at the primary PEZ layer $l^*=5$.

Concept pair	Angle (degrees)
Physics vs. motion direction	90.0°
Physics vs. random unit vector	85.0
Mean physics orthogonality	87.5

gests that layer 5 is where the relevant physics representation becomes available for intervention.

5.5. Per-Block CAV Disentanglement

We train separate CAVs for each IntPhys physics principle (O1/O2/O3) at the primary PEZ layer $l^*=5$ and measure pairwise angles using Eq. (7). Tab. 4 summarises probe accuracy and CAV angles.

The near-orthogonality of O2 and O3 (86.1°) suggests that continuity and solidity are encoded by largely independent directions, which supports principle-specific steering. O1 (object permanence) is less orthogonal to both (75.7 – 76.3°), consistent with the idea that permanence judgments partially overlap with continuity and solidity cues. These results show that VideoMAE encodes distinct physics principles as separable directions within PEZ representation space.

5.6. Subspace Orthogonality

We measure the angle between the physics CAV \mathbf{v}_{l^*} and other concept directions in the same representation space. Following Joseph *et al.* [7], we use motion direction as the reference concept (lateral motion, left vs. right) and a random unit vector as a baseline.

The physics CAV is orthogonal to motion direction (90.0°), higher than the 69 – 83° range reported by Joseph *et al.* One possible reason is that our CAV is trained on a balanced possible/impossible dataset, which may reduce motion-direction confounds.

The physics-vs.-random angle of 85.0° (rather than the expected ≈ 90) suggests that the CAV is a semantically structured direction rather than a random vector in high-dimensional space. This geometry indicates that steering physics need not directly interfere with motion direction, which makes compositional steering plausible.

Representation geometry. Fig. 5 shows UMAP projections of PEZ-layer activations for the test set. Possible (blue) and impossible (red) videos form partially separated clusters. After steering a possible video with $\alpha=+10$, its representation moves toward the impossible cluster along the learned CAV \mathbf{v}_{l^*} . The displacement scales with α and is sufficient to drive $P(\text{impossible})$ to 1.0 at $\alpha=+5$.

6. Conclusion

We presented physics steering, a method for controlling physical plausibility in a video world model at inference time. By extracting Concept Activation Vectors from linear probes at the Physics Emergence Zone (PEZ) of VideoMAE and injecting them into hidden states, we obtain bidirectional control of the model’s physics-related representations without updating model weights. Layer-specificity ablations localize this effect to the PEZ, while subspace analysis shows that physics and motion direction are orthogonal (90.0°). We also find that distinct physics principles (O1/O2/O3) are encoded as separable directions within the PEZ, with O2–O3 nearly orthogonal (86.1°). Together, these results suggest that physical reasoning in video models is not only readable, but also directly steerable at inference time.

7. Future Work

A natural next step is to connect representation-space steering to pixel-space generation by decoding steered latents into videos, which would make the effect of the intervention directly observable and could enable causal data augmentation for physical reasoning. A second direction is to move beyond a single uniform steering vector toward richer control, including steering along the full physics subspace, composing physics and motion controls, and applying interventions only at selected moments in time. Finally, it will be important to test the generality of these findings across datasets and video architectures, including whether similar physics directions and emergence zones appear beyond VideoMAE.

8. Broader Impact

Our method is model-agnostic: any video transformer with a localised physics subspace can be steered via the same CAV approach. Whether a PEZ exists in DINOv2 [13] on video, VideoGPT [20], or Stable Video Diffusion [1] is an open empirical question that our probing method-

ology can directly address. Physics steering can systematically stress-test world models by generating physically impossible scenarios without dataset collection, with clear value for AI safety evaluation. We note the dual-use risk that the same technique could produce physically incorrect but visually plausible content, and recommend that deployment in generative pipelines include a plausibility audit step.

References

- [1] Andreas Blattmann et al. Stable video diffusion: Scaling latent video diffusion models to large datasets. *arXiv preprint arXiv:2311.15127*, 2023. 6
- [2] Tim Brooks, Aleksander Holynski, and Alexei A. Efros. InstructPix2Pix: Learning to follow image editing instructions. In *IEEE/CVF Conference on Computer Vision and Pattern Recognition (CVPR)*, 2023. 2
- [3] Tim Brooks et al. Video generation models as world simulators. Technical report, OpenAI, 2024. 2
- [4] Agrim Gupta, Silvio Savarese, Surya Ganguli, and Li Fei-Fei. Embodied intelligence via learning and evolution. In *Advances in Neural Information Processing Systems (NeurIPS)*, 2021. 1
- [5] Danijar Hafner, Timothy Lillicrap, Mohammad Norouzi, and Jimmy Ba. Mastering Atari with discrete world models. In *International Conference on Learning Representations (ICLR)*, 2021. 1, 2
- [6] Anthony Hu, Lloyd Russell, Hudson Yeo, Zak Murez, George Fedoseev, Alex Kendall, Jamie Shotton, and Peter Corke. GAIA-1: A generative world model for autonomous driving. *arXiv preprint arXiv:2309.17080*, 2023. 1, 2
- [7] Sonia Joseph, Jack Lindsey, and Jack Lindsey. Interpreting physics in video world models. *Blog post*, 2024. 1, 2, 3, 6
- [8] Will Kay et al. The Kinetics human action video dataset. *arXiv preprint arXiv:1705.06950*, 2017. 4
- [9] Been Kim, Martin Wattenberg, Justin Gilmer, Carrie Cai, James Wexler, Fernanda Viegas, and Rory Sayres. Interpretability beyond classification with TCAV. In *International Conference on Machine Learning (ICML)*, 2018. 1, 2
- [10] Kenneth Li, Oam Patel, Fernanda Viégas, Hanspeter Pfister, and Martin Wattenberg. Inference-time intervention: Eliciting truthful answers from a language model. In *Advances in Neural Information Processing Systems (NeurIPS)*, 2023. 2
- [11] Jack Lindsey and David Bau. Sparse feature circuits: Discovering and editing interpretable causal graphs in language models. *arXiv preprint arXiv:2403.19647*, 2024. 2
- [12] Vincent Micheli, Eloi Alonso, and François Fleuret. Transformers are sample-efficient world models. In *International Conference on Learning Representations (ICLR)*, 2023. 1
- [13] Maxime Oquab et al. DINOv2: Learning robust visual features without supervision. *Transactions on Machine Learning Research (TMLR)*, 2024. 6
- [14] Luis S. Piloto, Ari Weinstein, Peter Battaglia, and Matthew Botvinick. Intuitive physics learning in a deep-learning model inspired by developmental psychology. *Nature Human Behaviour*, 2022. 2
- [15] Ronan Riochet, Mario Ynocente Castro, Mathieu Bernard, Adam Lerer, Rob Fergus, Véronique Izard, and Emmanuel Dupoux. IntPhys: A framework and benchmark for visual intuition physics. *arXiv preprint arXiv:1803.07616*, 2019. 2, 3
- [16] Ian Tenney, Dipanjan Das, and Ellie Pavlick. BERT rediscovers the classical NLP pipeline. In *Annual Meeting of the Association for Computational Linguistics (ACL)*, 2019. 2
- [17] Zhan Tong, Yibing Song, Jue Wang, and Limin Wang. VideoMAE: Masked autoencoders are data-efficient learners for self-supervised video pre-training. In *Advances in Neural Information Processing Systems (NeurIPS)*, 2022. 1, 4
- [18] Aaron van den Oord, Oriol Vinyals, and Koray Kavukcuoglu. Neural discrete representation learning. In *Advances in Neural Information Processing Systems (NeurIPS)*, 2017. 2
- [19] Zhouxia Wang, Ziyang Yuan, Xintao Wang, Yaowei Li, Tianshui Liu, Chun-Wei Zheng, and Enze Xie. MotionCtrl: A unified and flexible motion controller for video generation. In *ACM SIGGRAPH 2024*, 2024. 2
- [20] Wilson Yan, Yunzhi Zhang, Pieter Abbeel, and Aravind Srinivas. VideoGPT: Video generation using VQ-VAE and transformers. *arXiv preprint arXiv:2104.10157*, 2021. 2, 6
- [21] Mengjiao Yang, Yilun Du, Kamyar Ghasemipour, Jonathan Tompson, Bernhard Schölkopf, and Pieter Abbeel. Learning interactive real-world simulators. *arXiv preprint arXiv:2310.06114*, 2023. 1
- [22] Lvmin Zhang, Anyi Rao, and Maneesh Agrawala. Adding conditional control to text-to-image diffusion models. In *IEEE/CVF International Conference on Computer Vision (ICCV)*, 2023. 1, 2
- [23] Andy Zou, Long Phan, Sarah Chen, James Campbell, Phillip Guo, Richard Ren, Alexander Pan, Xuwang Yin, Mantas Mazeika, Ann-Kathrin Dombrowski, et al. Representation engineering: A top-down approach to AI transparency. *arXiv preprint arXiv:2310.01405*, 2023. 2